# Changes of signaling molecules in the axotomized rat facial nucleus

**Takashi Ishijima**
Soka University
**Kazuyuki Nakajima** ( nakajima@soka.ac.jp )
Soka University

**comment**

**Keywords:** facial nerve axotomy, motoneuron, microglia, c-Jun, CREB, MAPK

**Posted Date:** May 27th, 2022

**DOI:** https://doi.org/10.21203/rs.3.rs-1674940/v1

# Abstract

Axotomy of the rat facial nerve causes downregulation of motoneuron-specific molecules, including choline acetyltransferase and the vesicular acetylcholine transporter, in surviving motoneurons. Subsequently, resident microglia are activated and proliferate. These cellular responses are thought to promote the survival, repair and regeneration of motoneurons. However, it is still unclear which signaling molecules are involved in these responses. In this study, we investigated the changes and localizations of several signaling molecules, including immediate early genes (IEGs) such as c-Jun and c-Fos, transcription factors such as cAMP responsive element binding protein (CREB) and activating transcription factor 2 (ATF2), and mitogen-activated protein kinases (MAPKs) such as extracellular signal-regulated kinase (ERK)1/2, c-Jun N-terminal kinase (JNK) and p38. Immunoblotting and immunohistochemical analyses revealed the following. Among the IEGs, c-Jun was increased in injured motoneurons, but c-Fos did not respond to neuronal injury. Among the CREB/ATF family members, phosphorylated CREB (p-CREB) was significantly decreased in injured motoneurons. The levels of p-CREB/CREB and ATF2 were immunohistochemically increased in microglia. Among MAPKs, p-ERK1/2 and p-JNK1 were decreased in injured motoneurons at the late stage. p-p38 and p38 were markedly increased in microglia. In vitro experiments revealed that p38 and CREB were activated in proliferating microglia. These results strongly suggested that c-Jun is involved in the survival, repair and regeneration of motoneurons, but p-CREB/CREB, p-ERK/ERK and p-JNK/JNK are associated with the downregulation of motoneuron-specific molecules. On the other hand, p-p38/p38 and p-CREB/CREB were suggested to be closely involved in the activation/proliferation of microglia.


# Introduction

Facial nerve injury of adult rats leads to a variety of cellular responses in the axotomized facial nucleus (axotFN) [1]. Transection of the facial nerve triggers a reduction of functional molecules, such as choline acetyltransferase (ChAT), vesicular acetylcholine transporter (VAchT), m2 muscarinic acetylcholine receptor [2], and GABA receptor ($GABA_A$Ra1) [3]. In addition, microglia around the injured motoneuronal cell bodies begin to proliferate [4]. These cellular responses are thought to be mediated by specific signaling pathways after transection of the facial nerve. However, there are limited reports on the signaling pathways involved in these cellular changes. In this study, we investigated the changes in the levels and localization of several signaling molecules involved in the neuronal injury/repair/regeneration and glial responses. We selected c-Jun and c-Fos as representative immediate early genes (IEGs) that serve in early cellular responses [5]. From the CREB/ATF family, we chose cAMP response element binding protein (CREB), which is involved in neuronal differentiation, survival and function [6–8], and activating transcription factor 2 (ATF2), which is connected to anti-apoptotic actions [9]. We also selected extracellular signal-regulated kinase (ERK1/2), c-Jun N-terminal kinase (JNK), and p38 as representative mitogen-activated protein kinases (MAPKs), which are related to various cellular functions and in the nervous system [10, 11]. Our results showed that c-Jun was remarkably upregulated in injured motoneurons, but c-Fos was not changed. Phosphorylated CREB (p-CREB) was decreased in injured

motoneurons but increased in proliferating microglia. ATF2 was unchanged in injured motoneurons but increased in proliferating microglia. p-ERK1/2 and p-JNK were slightly decreased in injured motoneurons. On the other hand, p-p38 was increased in the proliferating microglia. In vitro experiments revealed that p38 and CREB in microglia were activated in response to macrophage-colony stimulating factor (M-CSF) stimulation, suggesting that the upregulations of p-p38 and p-CREB are related to the proliferation of microglia. These analyses revealed that facial nerve axotomy caused upregulation or downregulation of specific signaling molecules in the ipsilateral facial nucleus, and strongly suggested that these responses are intimately connected to motoneuronal survival, repair, regeneration and/or glial activation and proliferation.

# Materials And Methods

### Antibodies and miscellaneous

Anti-VAchT (sc-7717), anti-c-Jun (sc-1694), anti-b actin (sc-47778), anti-ATF2 (sc-6233), anti-mitogen and stress-activated kinase 1 (MSK1) (sc-9392) and anti-glial fibrillary acidic protein (GFAP) (sc-33673) antibodies were purchased from Santa Cruz Biotechnology (Dallas, TX). Another anti-c-Jun antibody (#PC06) for immunoblotting was purchased from Oncogene Science (Uniondale, NY). Anti-ChAT antibody (MAB5270) and anti-ChAT antibody (AB144P) were purchased from Millipore (Temecula, CA) and Sigma-Aldrich® (St. Louis, MO), respectively. Anti-c-Fos (#2250), anti-p-CREB (#9196), anti-CREB (#9197), anti-p-ERK1/2 (#4370), anti-ERK1/2 (#4695), anti-p-JNK (#4668), anti-JNK (#9258), anti-p-p38 (#9215), anti-p38 (#9212) and anti-p-MSK1 (#9591) antibodies were purchased from Cell Signaling Technology (Danvers, MA). An additional anti-p-CREB antibody (Y011052) for immunohistochemistry was purchased from abm® (Vancouver, Canada). An additional anti-p-JNK antibody (AF1205) for immunohistochemistry was purchased from R&D Systems (Minneapolis, MN). Anti-CD11b antibody (MCA275GA) was purchased from Bio-Rad (Hercules, CA).

Horseradish peroxidase (HRP)-conjugated anti-goat IgG (sc-2056) was purchased from Santa Cruz Biotechnology. HRP-conjugated anti-rabbit IgG (711-035-152), HRP-conjugated anti-mouse IgG (715-035-150), Alexa Fluor® 488 anti-rabbit IgG (711-545-152), Alexa Fluor® 488 anti-goat IgG (705-545-147) and Alexa Fluor® 594 anti-mouse IgG (715-585-150) were purchased from Jackson ImmunoResearch (West Grove, PA). Alexa Fluor® 488 anti-mouse IgG (A11001) and Alexa Fluor® 568 anti-rabbit IgG (A11011) were purchased from Life Technologies™ (Carlsbad, CA). Alexa Fluor® 568 anti-goat IgG (ab175704) was purchased from abcam (Cambridge, UK).

The ABC kit was purchased from Funakoshi (Tokyo). 3,3’ diaminobenzidine tetrahydrochloride (DAB) was purchased from Wako (Tokyo). VectaMount™ was obtained from Vector Laboratories (Burlingame, CA). ParmaFluor and Dulbecco’s modified Eagle medium (DMEM) were obtained from Thermo Fisher Scientific (Waltham, MA). Cresyl violet was supplied by Kanto Chemical (Tokyo). M-CSF (M9170) was obtained from Sigma-Aldrich®.

## Animals and surgery

Eight-week-old male Wistar rats (littermates) were used in this experiment. The rats were kept in an environment set to a 12-h light/dark cycle with free access to food and water. All animal experiments were conducted in compliance with the code of ethics of Soka University. The animal experiments were approved by the Ethics Committee of Soka University [approval codes: 19014 (2019), 20012 (2020), 21011 (2021)]. Under isoflurane anesthesia, the right facial nerve of rats was cut at the stylomastoid foramen. At 1.5, 3, 6, and 12 h, or 1, 3, 5, 7, and 14 d after axotomy, rats were decapitated under anesthesia, and the whole brains were removed and stored at -80°C until use.

For perfusion fixation of the brain, we performed a thoracotomy under anesthesia and perfused the brain transcardially with 200 mL of phosphate buffered saline (PBS) followed by 200 mL of 4% paraformaldehyde (PFA)/PBS. The de-bleached and fixed whole brains were removed and then post-fixed with 4% PFA/PBS. They were further immersed in 10%, 20%, and 30% sucrose solution, respectively, and stored at -80°C.

## Immunoblotting

The left (control side) and right (injury side) facial nuclei were cut out from the frozen brainstem, homogenized by non-reducing SDS lysis solution [62.5 mM Tris-HCl (pH 6.8), 2.3% SDS, 10% glycerol, 2 mM pyrophosphate, 2 mM NaF, 2 mM $Na_3VO_4$], and centrifuged (100,000 x g, 30 min). The supernatant was recovered and the protein amount was quantified by the Lowry method [12]. These samples were subjected to immunoblotting. The PVDF membrane was treated with blocking solution for 1 h, followed by the incubation of primary antibody at 4°C for 16 h. The primary antibodies were diluted as follows: c-Jun (1:1000), b-actin (1:2000), c-Fos (1:500), p-CREB (1:1000), CREB (1:1000), ATF2 (1:1000), p-ERK1/2 (1:1000), ERK1/2 (1:1000), p-JNK (1:1000), JNK (1:1000), p-p38 (1:1000), p38 (1:1000), p-MSK1 (1:1000) and MSK1 (1:1000). The staining methods were described previously [2].

## Immunohistochemistry

The brainstem was cut into 20 mm-thick sections with a Cryostat (Leica CM1860), and the sections were used for immunohistochemistry.

For ABC staining, we used a Vectastain® ABC kit. Brainstem sections were incubated with a primary antibody in blocking solution at 4°C for 16 h, then washed with 10 mM PBS (5 min x 2). The sections were then incubated with biotinylated secondary antibody for 2 h. After rinsing with 10 mM PBS, the avidin-biotin complex solution was reacted for 2 h at room temperature. Sections were colorized with a chromogenic DAB in 10 mM PBS. Colored sections were dehydrated in an ethanol series and sealed in VectaMount™.

For fluorescent staining, the sections were incubated with a primary antibody in blocking solution for 16 h at 4°C, and then reacted with a fluorescence labeled secondary antibody for 16 h at 4°C. After washing,

the sections were sealed with ParmaFluor.

For double staining, the sections were incubated with the first primary antibody at 4°C for 16 h. After washing, the sections were incubated with an appropriate secondary antibody at 4°C for 16 h. After that, the sections were incubated with the second primary antibody at 4°C for 16 h. The sections were then incubated with a suitable secondary antibody at 4°C for 16 h. These sections were sufficiently washed and mounted with PermaFluor.

### Nissl staining

Twenty mm-thick brainstem sections were used for Nissl staining. After air drying, the cryosections were dehydrated using an ethanol concentration series (30%, 50%, 70%, 95%, 100%) and then rehydrated using another ethanol concentration series (95%, 70%, 50%, and 30%). The sections were stained with 0.5% cresyl violet/1 M acetate buffer (pH 3.9) for 1 h. The sections were washed with running water, and then the specimens were dehydrated and sealed with VectaMount$^{TM}$.

### Preparation of microglia

Microglia were obtained from a primary culture that was prepared from newborn rat brains as described previously [13]. Briefly, microglia were floated by gentle shaking of primary mother cultures, and seeded on 60-mm dishes (Nunclon) at a density of 1.5 x $10^6$. The dishes were rinsed three times with serum-free DMEM and maintained with the same medium overnight.

The microglia in each dish were exposed to M-CSF (20 ng/mL), and recovered at 0, 5, 10, 15, and 30 min with phosphatase inhibitor solution [20 mM Tris-HCl (pH 7.4), 10 mM pyrophosphate, 10 mM NaF, 10 mM $Na_3VO_4$]. The collected cells were freeze-dried and solubilized with non-reducing SDS lysis solution. The cell homogenates were analyzed for p-p38/p38, p-CREB/CREB and p-MSK1/MSK1 by immunoblotting as described above.

### Statistical processing

The density of the bands in the Western blot was measured with Image J, and expressed as means ± SDs from three to five experiments. Differences between control and injured nuclei were evaluated by Student's t-test; In all cases, P values less than 0.05 were considered significant (*P < 0.05, **P < 0.01).

## Results

### Response of motoneurons to axotomy

The right facial nerve of adult rats was transected at the stylomastoid foramen (Fig. 1a, top), and at a suitable time point each brain was recovered. For immunoblotting, the left facial nucleus (Ct) and right facial nucleus (Op) were cut out from the brainstem (Fig. 1a, bottom), and for immunohistochemistry coronal cryosections of the brainstem were prepared.

Using the brainstem sections taken at 5 d post-insult, we immunohistochemically examined the changes of ChAT and VAchT. The immunohistochemical images showed that ChAT-expressing and VAchT-expressing cells were considerably decreased in the axotFN compared to the control nucleus (ctFN) (Fig. 1b, c). The quantified results indicated that the levels of ChAT and VAchT in the axotFN were decreased to 0.22 ± 0.21 (Fig. 1e) and 0.25 ± 0.07 (Fig. 1f), respectively. These results suggested that the axotomy of the facial nerve led to the downregulation of functional molecules for motoneurons.

Next, to clarify whether the downregulations of ChAT and VAchT were caused by the death of injured motoneurons, we performed Nissl staining (Fig. 1d). The results showed that the number of living motoneurons in the ctFN (Ct) was 133 ± 5 cells and the number in the axotFN (Op) was 127 ± 16 cells (Fig. 1g), indicating that there were no significant changes in the numbers of living motoneurons between ctFN and axotFN at 5 d post-insult. Thus, these results indicated that axotomy of the facial nerve caused the reduction of ChAT and VAchT levels in the injured but surviving facial motoneurons.

## Changes and localization of immediate early genes

### c-Jun

The levels of c-Jun in the axotFN were examined by immunoblot. The quantified levels of c-Jun in the axotFN were 1.01 ± 0.32, 0.91 ± 0.15, 1.10 ± 0.15, 1.70 ± 0.06, 1.78 ± 0.59, 2.10 ± 0.64, 3.31 ± 0.64, 2.39 ± 0.30, and 1.38 ± 0.26, at 1.5, 3, 6, and 12 h, and 1, 3, 5, 7, and 14 d post-insult, respectively (Fig. 2a, b). Thus, these results indicated that c-Jun in the axotFN was significantly increased from 12 h to 7 d.

To determine which cells increased the level of c-Jun in the axotFN, we immunohistochemically stained brainstem sections taken at 5 d post-insult. The results indicated that the number and the intensity of c-Jun expression were increased in axotFN compared to the ctFN (Fig. 2c). The dual staining with anti-ChAT antibody and anti-c-Jun antibody clarified that the c-Jun was present in the nucleus of anti-ChAT antibody-positive motoneurons (Fig. 2d). These results indicated that c-Jun was enhanced in injured facial motoneurons after the axotomy.

### c-Fos

We then analyzed the changes of c-Fos in axotFN by immunoblotting (Fig. 3a). Quantified results of c-Fos in axotFN were 1.08 ± 0.03, 1.03 ± 0.06, 0.97 ± 0.14, 0.97 ± 0.14, 0.96 ± 0.14, 0.89 ± 0.15, 1.00 ± 0.02, 1.06 ± 0.11, 0.97 ± 0.15, at 1.5, 3, 6, and 12 h, and 1, 3, 5, 7, and 14 d, respectively (Fig. 3b).

The immunohistochemical staining indicated that c-Fos was almost equally expressed in both nuclei, and there was no significant difference in c-Fos levels between the nuclei (Fig. 3c). Dual staining method indicated that c-Fos was localized in the nuclei of ChAT-expressing motoneurons (Fig. 3d). Collectively, these results indicated that c-Fos was homeostatically expressed in motoneurons, and the levels were not influenced by the transection.

## Changes and Localization of CREB/ATF family

### p-CREB and CREB

Immunoblotting indicated that the levels of p-CREB in axotFN were 0.18 ± 0.11, 0.22 ± 0.13, 0.14 ± 0.07, 0.22 ± 0.12, 0.12 ± 0.01, 0.10 ± 0.07, 0.08 ± 0.04, 0.20 ± 0.20, 0.20 ± 0.06 at 1.5, 3, 6, and 12 h, and 1, 3, 5, 7, and 14 d, respectively (Fig. 4a, b, p-CREB). These results indicated that active CREB significantly decreased from 1.5 h to 14 d in the axotFN. The quantified levels of CREB in axotFN were 1.13 ± 0.11, 0.98 ± 0.06, 1.18 ± 0.13, 1.10 ± 0.19, 1.39 ± 0.07, 1.50 ± 0.13, 1.65 ± 0.17, 1.72 ± 0.21, 1.70 ± 0.19 at 1.5, 3, 6, and 12 h, and 1, 3, 5, 7, and 14 d, respectively (Fig. 4a, b, CREB), indicating that the CREB was increased at a later stage (1–14 d post-insult).

The ABC immunohistochemical method showed that p-CREB was stained as large and small points in the ctFN, but the large points were lost and only small points remained in the axotFN (Fig. 4c, p-CREB). The number of small p-CREB-positive points was increased in the axotFN compared to the ctFN. CREB was stained as large points and small points in both nuclei, but there were more small points in the axotFN than the ctFN (Fig. 4c, CREB). Double staining method showed that the large CREB-positive points were consistent with the nuclei of ChAT-positive motoneurons (Fig. 4d), and the small CREB-positive points corresponded to the nuclei of CD11b-positive microglia (Fig. 4d). The CREB-staining was not entirely consistent with GFAP-positive astrocytes (Fig. 4d). Therefore, we can say that CREB is highly activated as p-CREB in normal motoneurons and microglia, but the active p-CREB would be markedly inactivated upon transection of motoneurons.

### ATF2

Immunoblotting for ATF2 indicated the levels of ATF2 in the axotFN were 0.93 ± 0.09, 0.95 ± 0.28, 1.07 ± 0.18, 0.96 ± 0.08, 1.02 ± 0.08, 0.82 ± 0.05, 1.03 ± 0.23, 0.94 ± 0.10, 1.05 ± 0.14 at 1.5, 3, 6, and 12 h, and 1, 3, 5, 7, and 14 d, respectively (Fig. 5a, b), implying that motoneuron axotomy did not significantly influence the level of ATF2 in the axotFN.

By the ABC method, ATF2 was observed as large and small points in both nuclei (Fig. 5c). However, we found that there was a greater number of small ATF2-positive points in the axotFN compared to the ctFN, although there was no significant difference in the number of large ATF2-positive points between the axotFN and ctFN (Fig. 5c). Dual staining with ChAT, CD11b, and GFAP antibodies indicated that the large ATF2-positive points were consistent with the nuclei of ChAT-positive motoneurons, and the small ATF2-positive points coincided with the nuclei of CD11b-positive microglia (Fig. 5d), but not those of GFAP-positive astrocytes (Fig. 5d). These results indicated that ATF2 in the motoneurons was not affected by axotomy, but the increase of ATF2 in microglia was associated with the proliferation occurring around injured motoneurons at this time.

## Changes of MAPK in the axotomized facial nucleus

### p-ERK1/2 and ERK1/2

As shown in Fig. 6a, p-ERK1/2 tended to decrease at 1–14 d in the axotFN. The quantification indicated that the levels of p-ERK1/2 in the axotFN were 0.89 ± 0.08, 1.06 ± 0.07, 1.02 ± 0.08, 0.74 ± 0.05, 0.65 ± 0.13, 0.43 ± 0.08, 0.41 ± 0.12, 0.38 ± 0.03, 0.33 ± 0.01 at 1.5, 3, 6, and 12 h, and 1, 3, 5, 7, and 14 d, respectively (Fig. 6b, p-ERK1/2). These results indicated that p-ERK1/2 was significantly decreased from 12 h to 14 d on the axotFN. The levels of ERK1/2 in the axotFN were 1.01 ± 0.04, 1.02 ± 0.04, 1.02 ± 0.15, 1.01 ± 0.08, 1.31 ± 0.06, 1.31 ± 0.08, 1.55 ± 0.15, 1.82 ± 0.20, 1.44 ± 0.16 at 1.5, 3, 6, and 12 h, and 1, 3, 5, 7, and 14 d, respectively, indicating that ERK1/2 increased at 1–14 d after injury (Fig. 6b, ERK1/2).

Immunohistochemical staining indicated that anti-p-ERK1/2 antibody stained many cells in the ctFN, but the staining of cells was weaker in the axotFN (Fig. 6c, p-ERK). On the other hand, the number of anti-ERK1/2 antibody-positive motoneurons in the axotFN was higher than that in ctFN (Fig. 6c, ERK1/2). The results of double staining indicated that the ERK1/2-expressing cells coincided with ChAT-expressing cells, suggesting that the ERK1/2-expressing cells were motoneurons (Fig. 6d).

## p-JNK and JNK

Immunoblotting indicated that the levels of p-JNK in the axotFN were 1.06 ± 0.16, 0.74± 0.28, 0.55 ± 0.04, 0.69 ± 0.16, 0.63 ± 0.02, 0.51 ± 0.09, 0.52 ± 0.13, 0.50 ± 0.17, 0.32 ± 0.18 at 1.5, 3, 6, and 12 h, and 1, 3, 5, 7, and 14 d, respectively (Fig. 7a, b, p-JNK). These results indicated that p-JNK1 was significantly decreased at 6 h to 14 d (Fig. 7B). On the other hand, the level of JNK in the axotFN were 1.03 ± 0.08, 1.06 ± 0.07, 1.02 ± 0.01, 1.07 ± 0.06, 0.70 ± 0.07, 0.66 ± 0.08, 0.70 ± 0. 05, 0.87 ± 0.10, 0.85 ± 0.12 at 1.5, 3, 6, and 12 h, and 1, 3, 5, 7, and 14 d, respectively (Fig. 7a, b, JNK), indicating that JNK in the axotFN was slightly but significantly decreased at 1–5 d.

In immunohistochemical staining, we could see many p-JNK-expressing large structures in the ctFN, but the number of such structures was decreased in the axotFN (Fig. 7c). Dual staining method demonstrated that p-JNK-expressing structures were localized in ChAT-expressing motoneurons (Fig. 7d). These results indicated that JNK1/2 was normally expressed in motoneurons and the levels transiently decreased at 1–5 d post-insult when motoneurons were transected. Most of the p-JNK in the facial motoneurons was p-JNK1, rather than p-JNK2, and the levels were significantly declined at 6 h to 14 d post-insult (Fig. 7a, b).

## p-p38 and p38

Finally, we analyzed the changes of p-p38 and p38 in the axotFN (Fig. 8a). Immunoblotting indicated that the levels of p-p38 in the axotFN were 0.79 ± 0.18, 0.43 ± 0.04, 0.49 ± 0.13, 0.64 ± 0.21, 1.36 ± 0.21, 1.65 ± 0.25, 2.21 ± 0.30, 4.11 ± 0.60, 3.40 ± 0.71 at 1.5, 3, 6, and 12 h, and 1, 3, 5, 7, and 14 d, respectively (Fig. 8b, p-p38). These results indicated that p-p38 was significantly decreased from 3 h to 12 h after injury, but then significantly increased from 1 d to 14 d. On the other hand, the levels of p38 in the axotFN were 1.15 ± 0.18, 1.10 ± 0.11, 0.99 ± 0.12, 1.08 ± 0.06, 1.51 ± 0.30, 1.90 ± 0.15, 2.36 ± 0. 17, 1.90 ± 0.07, 1.51 ± 0.08 at 1.5, 3, 6, and 12 h, and 1, 3, 5, 7, and 14 d, respectively (Fig. 8b, p38), indicating that p38 increased significantly from 3 to 14 d post-insult.

The immunohistochemical method indicated that p-p38-positive small cells were enhanced in the axotFN (Fig. 8c, p-p38). On the other hand, anti-p38 antibody stained both large cells and small cells in the ctFN (Fig. 8c, p38), and the number of anti-p38 antibody-positive cells was enhanced in the axotFN (Fig. 8c, p38). Dual staining with anti-p-p38/anti-CD11b antibodies clarified that p-p38 was colocalized with CD11b-expressing microglia (Fig. 9a). On the other hand, dual staining with anti-p-p38/anti-GFAP antibodies indicated that p-p38 staining was not colocalized with GFAP-staining (Fig. 9a).

We next examined which cell types expressed p38 by using double staining method. p38 was detected in both large cells and small cells (Fig. 9b). The p38-expressing large cells coincided with ChAT-expressing cells (Fig. 9b, top panels), suggesting that p38 was present in motoneurons. On the other hand, p38-expressing small cells coincided with CD11b-positive cells (Fig. 9b, medium panels), but not GFAP-positive cells (Fig. 9b, bottom panels), suggesting that p-38-expressing small cells were microglia.

### Phosphorylation of p38 and CREB in M-CSF-stimulated microglia

Detection of p-p38 and p-CREB in microglia in the axotFN allowed us to predict that p38 and CREB were phosphorylated by stimulus with microglial mitogen M-CSF. Thus, we examined in vitro whether p38 and CREB in microglia are activated by M-CSF. Immunoblotting showed that p38 and CREB were rapidly phosphorylated by stimulus with M-CSF (Fig. 10a, b). In addition, MSK1 was found to be phosphorylated in M-CSF-stimulated microglia (Fig. 10c). The amounts of b-actin were constant (Fig. 10d). These results strongly suggest that p38, CREB and MSK1 are phosphorylated in proliferating microglia in vivo.

## Discussion

### Response of IEGs to nerve injury

Transection of the facial nerve of adult rats resulted in a functional decrease of motoneurons and glial activation/proliferation [2, 3, 14]. This fact allowed us to speculate that some specific signaling molecules/transcription factors play a role in such phenomena in the axotFN. As a possible candidate, we first analyzed IEGs. The IEGs c-Jun and c-Fos are generally known to form a dimer as AP-1, which acts as a transcriptional regulator [15, 16], and thus we examined the change in the quantity of c-Jun and c-Fos over a time course (Table 1).

The results showed that c-Jun levels were significantly increased in injured facial motoneurons after 12 h post-insult (Fig. 2), suggesting that the elevated c-Jun level upregulated the formation of c-Jun/c-Fos and the increased levels of AP-1 promoted the transcription of specific genes for neuronal regeneration. Herdegen et al. [17] observed that c-Jun is induced in the injured dorsal root ganglia, motoneurons and dorsal horn in the rat sciatic nerve injury system, and they further described that c-Jun is related to neuronal protection and regeneration in the adult nervous system [18]. Raivich et al. [19] also reported that c-Jun is essential for axonal regeneration in the mouse facial nerve injury system. These reports and our results suggest that c-Jun is involved in a regulatory pathway of the neuronal regeneration.

c-Fos has been little studied at the protein level, and its presence, induction/reduction and function in injured neurons remain largely unexplained. Haas et al. [20] described that c-Fos mRNA was not detected in the axotFN. In contrast to their results, we detected c-Fos protein in the rat facial nucleus, and demonstrated that c-Fos is present in motoneurons in constant amounts and the levels hardly fluctuate by facial nerve axotomy (Fig. 3). We originally predicted that c-Fos and c-Jun are both upregulated, and thus the formed AP-1 (c-Jun/c-Fos) would also be upregulated in the axotFN. However, our present experiments demonstrated that c-Jun alone was induced in facial motoneurons by axotomy (Fig. 2,3). This might suggest that the formation of AP-1 in injured facial motoneurons is regulated by the upregulation/downregulation of the c-Jun level, but not the c-Fos level.

### Response of the CREB/ATF family to nerve injury

The CREB/ATF family members are known to play an important role in a wide variety of neurofunctions, such as activity-dependent transcription, plasticity, memory, and survival of neurons [21]. We found that the level of CREB was increased in the axotFN from 1 d post-insult, but the level of p-CREB was severely decreased from 1.5 h post-insult (Fig. 4) (Table 1). These results suggested that the CREB activity was decreased in motoneurons, and thereby the CREB-mediated transcriptional activity was reduced and functional downregulation was induced in motoneurons. In a potentially related study, we previously reported that $GABA_A$Ra1 is markedly reduced in axotomized facial motoneurons [3]. Hu et al. [22] reported that the expression of $GABA_A$Ra1 is regulated by CREB in primary rat neocortical cultures. Thus, CREB activity would play the important role of regulating the levels of functional molecules in motoneurons. Generally, CREB is activated through the cAMP-dependent protein kinase (PKA) pathway, PKC-related pathway, and MAPK pathways [23, 24]. Thus, any of these pathways might be implicated in the downregulation of CREB in injured motoneurons in our system. However, among them it is most likely that p-ERK1/2 is linked to CREB activation, because the levels of p-ERK1/2 were significantly decreased in injured motoneurons (Fig. 6).

Interestingly, our immunohistochemical analysis demonstrated that p-CREB/CREB-expressing microglia were increased at the periphery of axotomized facial motoneurons, although this result was not reflected in the results of immunoblotting (Fig. 4). This finding suggested that CREB in microglia was relevant to microglial proliferation, which occurred at this time point (5 d post-insult).

ATF2 is a transcription factor associated with various cellular responses, such as anti-apoptosis, cell growth, and DNA damage. In our experiments, ATF2 was expressed in a constant amount in the nuclei of motoneurons, but it was not responsive to neuronal axotomy (Fig. 5) (Table 1).

However, immunohistochemical analysis indicated that ATF2-expressing microglia were increased in the axotFN (Fig. 5C). This naturally poses the question: What role do these ATF2-expressing microglia play? Li et al. [25] reported that ATF2 is induced and activated in microglia by lipopolysaccharide (LPS) stimulation both in vivo and in vitro, suggesting that ATF2 participates in microglial activation.

### Response of MAPKs to nerve injury

MAPKs are a family of Ser/Thr kinases that are involved in many biological phenomena, such as metabolism, cell growth, differentiation, and proliferation. ERK1/2 is activated by various factors and transduces signals to transcription factors [26, 27]. ERK was reported to serve in axonal regrowth in sciatic nerve-crushed rats [28] and in nerve survival and regeneration in a sciatic nerve axotomy model [29]. In our experiment, p-ERK1/2 was downregulated and ERK1/2 upregulated in axotomized facial motoneurons (Fig. 6a, b) (Table 1). These results suggested that the activation of ERK1/2 was inhibited by stimulus/stress due to facial nerve injury, and the reduced p-ERK1/2 levels would in turn suppress the activity of various downstream transcriptional regulators, including CREB (Fig. 4).

The second MAPK, JNK, is regarded as a stress-responsive MAPK. There are reports in which JNK was found to participate in axonal regeneration and neuronal development [30, 31]. However, in our injury system, p-JNK levels in the axotFN were found to gradually decrease with time (Fig. 7) (Table 1). Since the levels of decrease were significant but not particularly high, p-JNK may function to some extent in the tissue as an active JNK. At any rate, in our experiments the active JNK level decreased slightly in the axotFN (Fig. 7), but p-JNK was present at some level in the motoneuronal nuclei (Fig. 7), suggesting that JNK plays roles in injured motoneurons. Given these facts, it is plausible that neither a strong stress reaction nor an inflammatory reaction occurs in the axotFN.

The third MAPK, p38, is a Ser/Thr kinase that is activated by inflammatory cytokines, LPS, growth factors, and cellular stress. Nix et al. [32] reported that both p38 and JNK are required for the axonal regeneration of GABAergic neurons in *C. elegans*. However, we suggested that p-p38/p38 are involved in the microglial proliferation in vivo (Fig. 8c, Fig. 9) (Table 1). In fact, an in vitro study indicated that p38 was activated in M-CSF-stimulated microglia [14]. What molecules function downstream of p38 in microglia? One candidate is protein kinase MSK1. Since MSK1 is involved in the phosphorylation of CREB [33], we predicted that MSK1 and CREB are phosphorylated in M-CSF-stimulated microglia, and examined this possibility in vitro. Our results showed that MSK1 and CREB as well as p38 were actually phosphorylated in M-CSF-stimulated microglia (Fig. 10). This strongly suggests that the p38-MSK1/CREB cascade is involved in the reaction of microglial proliferation. p-38 was detected in motoneurons as well as microglia in the axotFN (Fig. 8c). However, p-p38 was not observed in motoneurons. Currently, the significance of the presence of p38 in motoneurons is not known. Taking these results together, we can say that the activation of p38 in microglia in the axotFN is closely associated with the activation/proliferation reactions rather than the inflammation and the immune reactions.

# Conclusion

In conclusion, c-Jun was suggested to be related to the transcription of survival- and repair-related genes in motoneurons, and p-CREB, p-ERK, and p-JNK were suggested to be associated with downregulation of motoneuron-specific molecules such as ChAT. On the other hand, p-CREB and p-p38 in microglia were predicted to be linked to the activation/proliferation reactions.

# Declarations

### Funding

This research was not supported by any specific grant from funding agencies in the public, commercial, or not-for-profit sectors.

### Author contributions

TI performed the operation on the animals and was primarily responsible for analyzing the signaling molecules by immunoblotting and immunohistochemistry. KN participated in designing the study and performed some supporting experiments.

### Conflict of interest

The authors declare that they have no conflict or competing interests.

## References

1. Moran LB, Graeber MB (2004) The facial nerve axotomy model. Brain Res Rev 44:154–178. https://doi.org/10.1016/j.brainresrev.2003.11.004
2. Ichimiya T, Yamamoto S, Honda Y et al (2013) Functional down-regulation of axotomized rat facial motoneurons. Brain Res 1507:35–44. https://doi.org/10.1016/j.brainres.2013.02.044
3. Kikuchi R, Hamanoue M, Koshimoto M et al (2018) Response of the GABAergic system to axotomy of the rat facial nerve. Neurochem Res 43:324–339. https://doi.org/10.1007/s11064-017-2427-1
4. Yamamoto S, Nakajima K, Kohsaka S (2010) Macrophage-colony stimulating factor as an inducer of microglial proliferation in axotomized rat facial nucleus. J Neurochem 115:1057–1067. https://doi.org/10.1111/j.1471-4159.2010.06996.x
5. Sng JCG, Taniura H, Yoneda Y (2004) A tale of early response genes. Biol Pharm Bull 27:606–612. https://doi.org/10.1248/BPB.27.606
6. Amidfar M, de Oliveira J, Kucharska E et al (2020) The role of CREB and BDNF in neurobiology and treatment of Alzheimer's disease. Life Sci 257:118020. https://doi.org/10.1016/j.lfs.2020.118020
7. Carlezon WA, Duman RS, Nestler EJ (2005) The many faces of CREB. Trends Neurosci 28:436–445. https://doi.org/10.1016/j.tins.2005.06.005
8. Landeira BS, Santana TTDS, Araújo JADM et al (2018) Activity-independent effects of CREB on neuronal survival and differentiation during mouse cerebral cortex development. Cereb Cortex 28:538–548. https://doi.org/10.1093/cercor/bhw387
9. Yuan Z, Gong S, Luo J et al (2009) Opposing roles for ATF2 and c-Fos in c-Jun-mediated neuronal apoptosis. Mol Cell Biol 29:2431–2442. https://doi.org/10.1128/MCB.01344-08
10. Liu MG, Wang RR, Chen XF et al (2011) Differential roles of ERK, JNK and p38 MAPK in pain-related spatial and temporal enhancement of synaptic responses in the hippocampal formation of rats:

Multi-electrode array recordings. Brain Res 1382:57–69. https://doi.org/10.1016/j.brainres.2011.01.076

11. Thomas GM, Huganir RL (2004) MAPK cascade signalling and synaptic plasticity. Nat Rev Neurosci 5:173–183. https://doi.org/10.1038/nrn1346
12. Lowry OH, Rosebrough NJ, Farr AL, Randall RJ (1951) Protein measurement with the folin phenol reagent. J Biol Chem 193:265–275. https://doi.org/10.1016/s0021-9258(19)52451-6
13. Oshiro S, Kawamura K, ichi, Zhang C et al (2008) Microglia and astroglia prevent oxidative stress-induced neuronal cell death: Implications for aceruloplasminemia. Biochim Biophys Acta - Mol Basis Dis 1782:109–117. https://doi.org/10.1016/J.BBADIS.2007.12.002
14. Yamamoto S, Kohsaka S, Nakajima K (2012) Role of cell cycle-associated proteins in microglial proliferation in the axotomized rat facial nucleus. Glia 60:570–581. https://doi.org/10.1002/glia.22291
15. Karin M, Liu ZG, Zandi E (1997) AP-1 function and regulation. Curr Opin Cell Biol 9:240–246. https://doi.org/10.1016/S0955-0674(97)80068-3
16. Rauscher FJ, Voulalas PJ, Franza BR, Curran T (1988) Fos and Jun bind cooperatively to the AP-1 site: reconstitution in vitro. Genes Dev 2:1687–1699. https://doi.org/10.1101/gad.2.12b.1687
17. Herdegen T, Fiallos-Estrada CE, Schmid W et al (1992) The transcription factors c-JUN, JUN D and CREB, but not FOS and KROX-24, are differentially regulated in axotomized neurons following transection of rat sciatic nerve. Mol Brain Res 14:155–165. https://doi.org/10.1016/0169-328X(92)90170-G
18. Herdegen T, Skene P, Bähr M (1997) The c-Jun transcription factor - bipotential mediator of neuronal death, survival and regeneration. Trends Neurosci 20:227–231. https://doi.org/10.1016/S0166-2236(96)01000-4
19. Raivich G, Bohatschek M, Da Costa C et al (2004) The AP-1 transcription factor c-Jun is required for efficient axonal regeneration. Neuron 43:57–67. https://doi.org/10.1016/j.neuron.2004.06.005
20. Haas CA, Donath C, Kreutzberg GW (1993) Differential expression of immediate early genes after transection of the facial nerve. Neuroscience 53:91–99. https://doi.org/10.1016/0306-4522(93)90287-P
21. Cox LJ, Hengst U, Gurskaya NG et al (2008) Intra-axonal translation and retrograde trafficking of CREB promotes neuronal survival. Nat Cell Biol 10:149–159. https://doi.org/10.1038/ncb1677
22. Hu Y, Lund IV, Gravielle MC et al (2008) Surface expression of GABAA receptors is transcriptionally controlled by the interplay of camp-response element-binding protein and its binding partner inducible camp early repressor. J Biol Chem 283:9328–9340. https://doi.org/10.1074/jbc.M705110200
23. Deisseroth K, Tsien RW (2002) Dynamic multiphosphorylaton passwords for activity-dependent gene expression. Neuron 34:179–182. https://doi.org/10.1016/s0896-6273(02)00664-5
24. Koga Y, Tsurumaki H, Aoki-Saito H et al (2019) Roles of cyclic AMP response element binding activation in the ERK1/2 and p38 MAPK signalling pathway in central nervous system,

cardiovascular system, osteoclast differentiation and mucin and cytokine production. Int J Mol Sci 20:1–23. https://doi.org/10.3390/ijms20061346

25. Li M, Zhang D, Ge X et al (2019) TRAF6-p38/JNK-ATF2 axis promotes microglial inflammatory activation. Exp Cell Res 376:133–148. https://doi.org/10.1016/j.yexcr.2019.02.005
26. Cargnello M, Roux PP (2011) Activation and function of the MAPKs and their substrates, the MAPK-activated protein kinases. Microbiol Mol Biol Rev 75:50–83. https://doi.org/10.1128/mmbr.00031-10
27. Rubinfeld H, Seger R (2005) The ERK cascade: A prototype of MAPK signaling. Mol Biotechnol 31:151–174. https://doi.org/10.1385/MB:31:2:151
28. Yamazaki T, Sabit H, Oya T et al (2009) Activation of MAP kinases, Akt and PDGF receptors in injured peripheral nerves. J Peripher Nerv Syst 14:165–176. https://doi.org/10.1111/j.1529-8027.2009.00228.x
29. Agthong S, Kaewsema A, Tanomsridejchai N, Chentanez V (2006) Activation of MAPK ERK in peripheral nerve after injury. BMC Neurosci 7:1–8. https://doi.org/10.1186/1471-2202-7-45
30. Kawasaki A, Okada M, Tamada A et al (2018) Growth cone phosphoproteomics reveals that GAP-43 phosphorylated by JNK is a marker of axon growth and regeneration. iScience 4:190–203. https://doi.org/10.1016/j.isci.2018.05.019
31. Schellino R, Boido M, Vercelli A (2019) JNK signaling pathway involvement in spinal cord neuron development and death. Cells 8. https://doi.org/10.3390/cells8121576
32. Nix P, Hisamoto N, Matsumoto K, Bastiani M (2011) Axon regeneration requires coordinate activation of p38 and JNK MAPK pathways. Proc Natl Acad Sci U S A 108:10738–10743. https://doi.org/10.1073/pnas.1104830108
33. Reyskens KMSE, Arthur JSC (2016) Emerging roles of the mitogen and stress activated kinases MSK1 and MSK2. Front Cell Dev Biol 4:1–8. https://doi.org/10.3389/fcell.2016.00056

# Tables

Table 1 is available in the Supplemental Files section.

# Figures

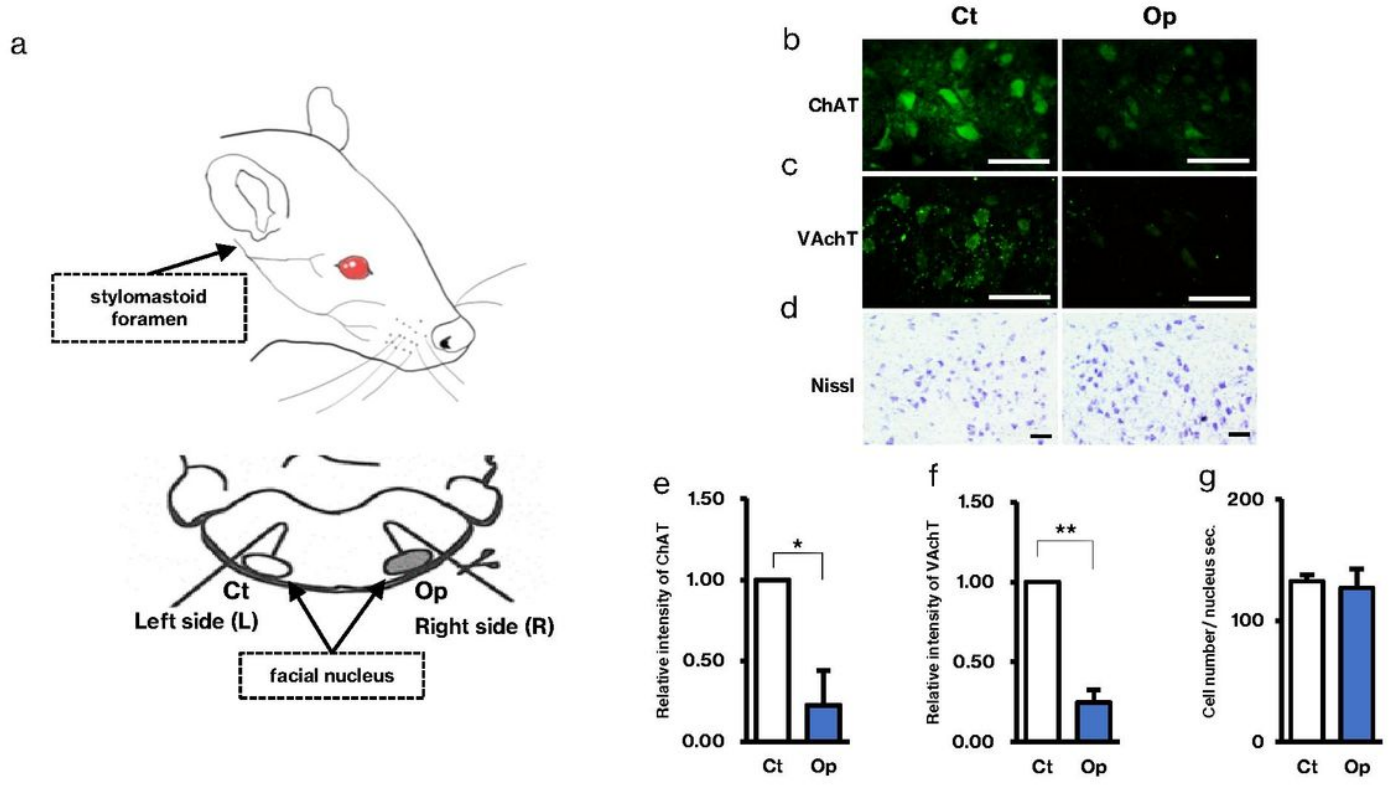


## Figure 1

### Functional downregulation and survivability of motoneurons

a. Axotomy of the rat facial nerve. The facial nerve of adult rats was unilaterally cut at the stylomastoid foramen. In this study, the right facial nerve was transected and the left facial nerve remained as a control. For immunohistochemical study, coronal cryosections were prepared at the depth of the facial nucleus in the brainstem, and for immunoblotting analysis each facial nucleus was cut out at a suitable time point.

b, c. Immunohistochemistry for ChAT and VAchT. Brainstem sections were stained with anti-ChAT antibody (b) and anti-VAchT antibody (c), and the control nucleus (Ct) and operated nucleus (Op) were compared. A typical result is shown. Scale bar = 100 μm.

d. Nissl staining. Brainstem sections taken at 5 d post-insult were stained by the Nissl staining method. A typical photo is shown. Scale bar = 100 μm.

e, f. Comparison of ChAT (e) and VAchT (f) intensities between the control nucleus (Ct) and operated nucleus (Op). The data shown are means ± SDs from four independent experiments (*P < 0.05, **P < 0.01).

g. Comparison of surviving motoneurons in both facial nuclei. The cell numbers in the control nucleus (Ct) and operated nucleus (Op) were counted by densitometry. The data shown are means ± SDs from three independent experiments (*P < 0.05, **P < 0.01).

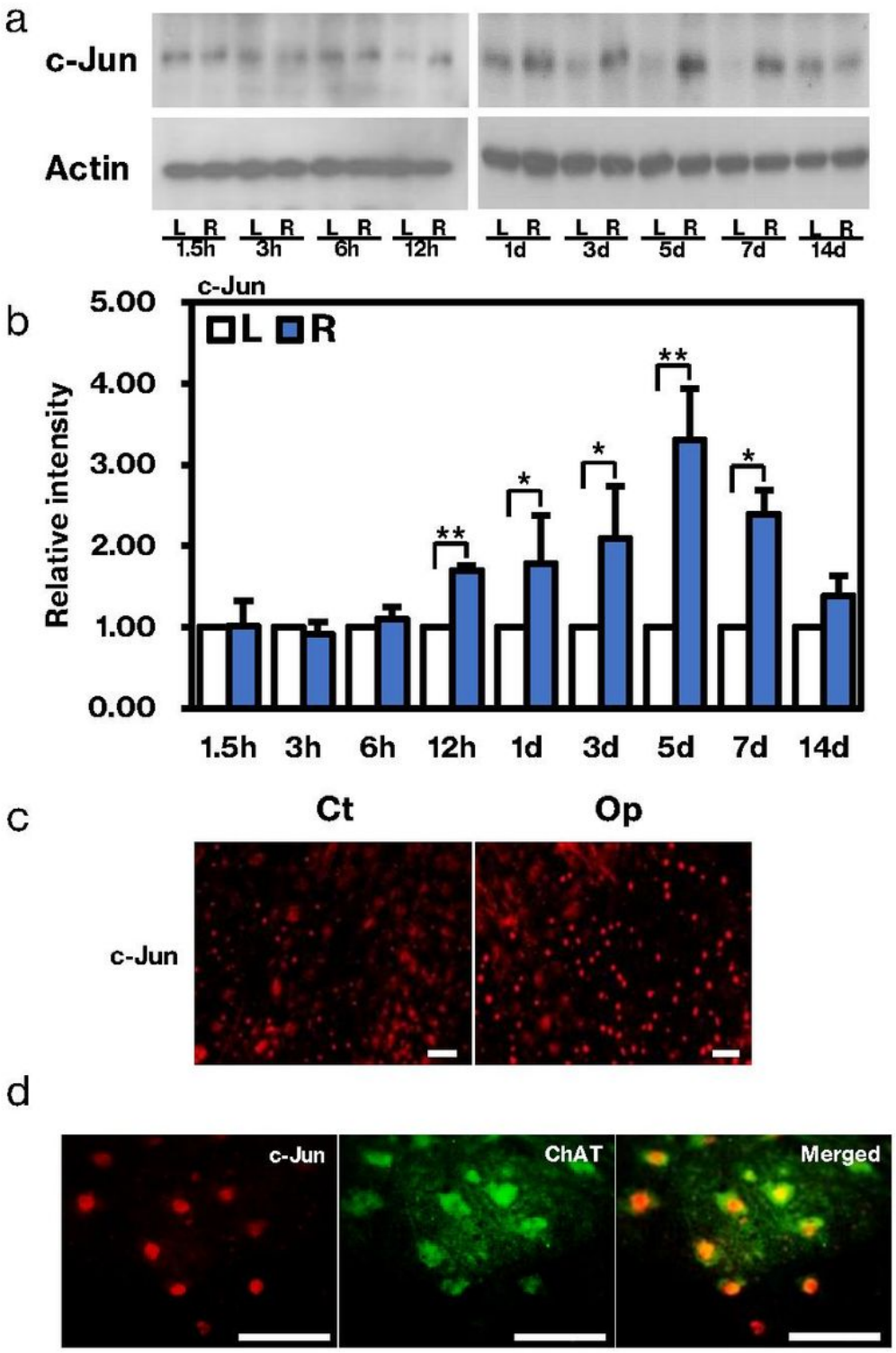


## Figure 2

### Changes of c-Jun in the axotomized facial nucleus

a. Immunoblotting for c-Jun. Tissue extracts of the control nucleus (L) and axotomized nucleus (R) taken at 1.5, 3, 6, and 12 h and 1, 3, 5, 7, and 14 d were analyzed by immunoblot for c-Jun (c-Jun) and actin (Actin).

b. Quantitative analysis of c-Jun. The intensities of the c-Jun bands were determined by densitometry and expressed as a value relative to that of the control nucleus (defined as 1.00). The data shown are means ± SDs from three to five independent experiments. Differences between the control nucleus (L) and operated nucleus (R) were assessed by Student's t-test (*P < 0.05, **P < 0.01).

c. Immunohistochemistry for c-Jun. Brainstem sections taken at 5 d post-insult were stained with anti-c-Jun antibody, and the control (Ct) and operated (Op) facial nucleus were compared. The scale bars are 100 μm.

d. Double staining with anti-c-Jun antibody and anti-ChAT antibody. Brainstem sections were dually stained for c-Jun (c-Jun) and ChAT (ChAT). Anti-c-Jun antibody-positive cells and anti-ChAT antibody-positive cells were visualized by Alexa Fluor-568 (red) and Alexa Fluor-488 (green), respectively. The merged image is shown on the right-hand side (Merged). The scale bar is 100 μm.

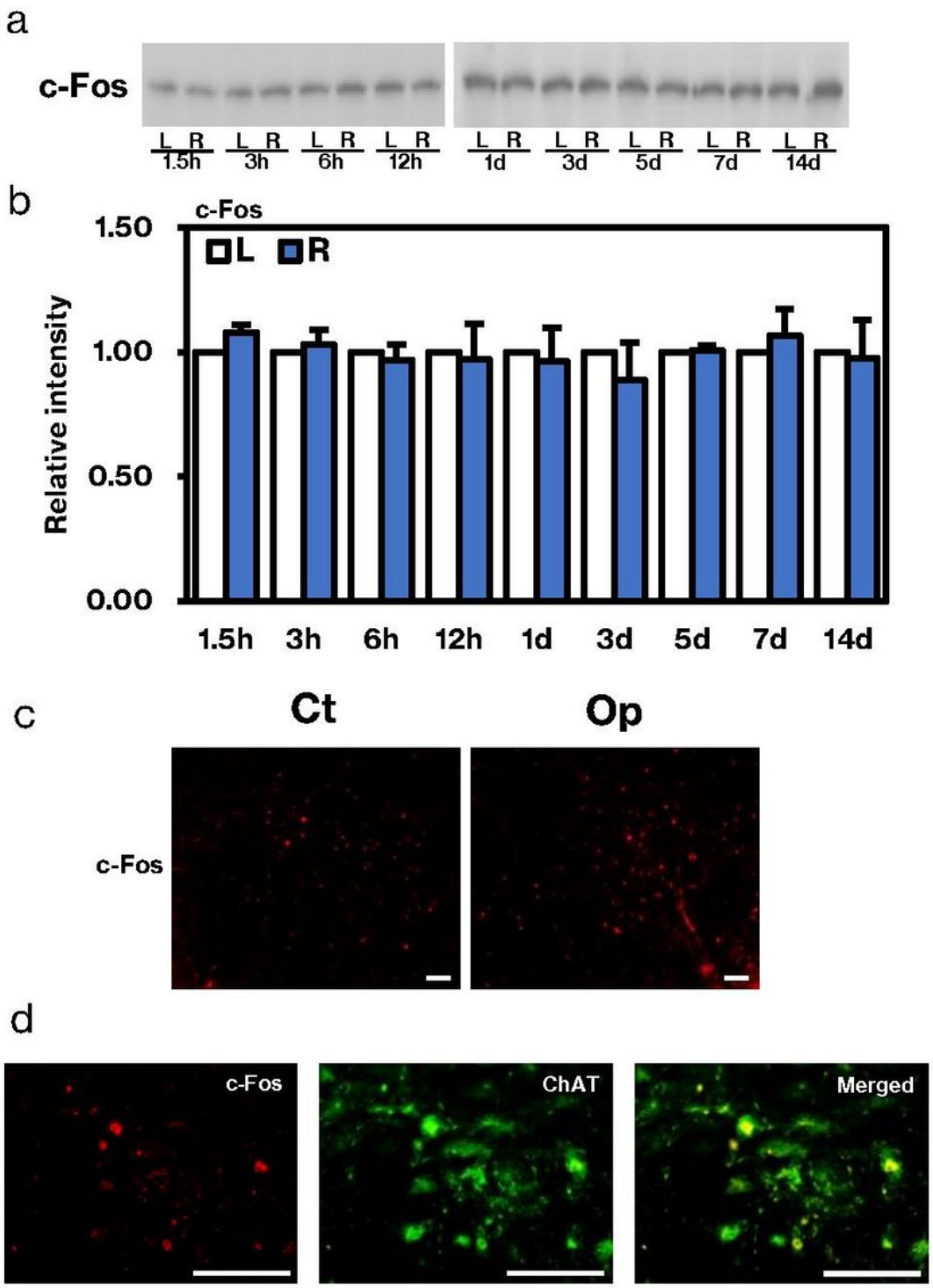


## Figure 3

### Changes of c-Fos in the axotomized facial nucleus

a. Immunoblot for c-Fos. Facial nucleus extracts taken at 1.5 h to 14 d post-insult were analyzed by immunoblotting for c-Fos. At each time point, the contralateral (L) and ipsilateral (R) nuclei were compared.

b. Quantitative analysis of c-Fos. The intensities of the c-Fos bands were determined by densitometry and were expressed as a value relative to that of the contralateral nucleus (defined as 1.00). The data shown are means ± SDs from three independent experiments. Differences between the control nucleus (L) and operated nucleus (R) were assessed by Student's t-test (*P < 0.05, **P < 0.01).

c. Immunohistochemistry for c-Fos. Brainstem sections taken at 5 d post-insult were stained with anti-c-Fos antibody, and the control (Ct) and operated (Op) nucleus are shown. The scale bar is 100 μm.

d. Double staining with anti-c-Fos antibody and anti-ChAT antibody. Brainstem sections at 5 d post-insult were dually stained with anti-c-Fos antibody and anti-ChAT antibody. c-Fos and ChAT were visualized by Alexa Fluor-568 (red) and Alexa Fluor-488 (green), respectively. The merged image is shown on the right-hand side (Merged). The scale bar is 100 μm.

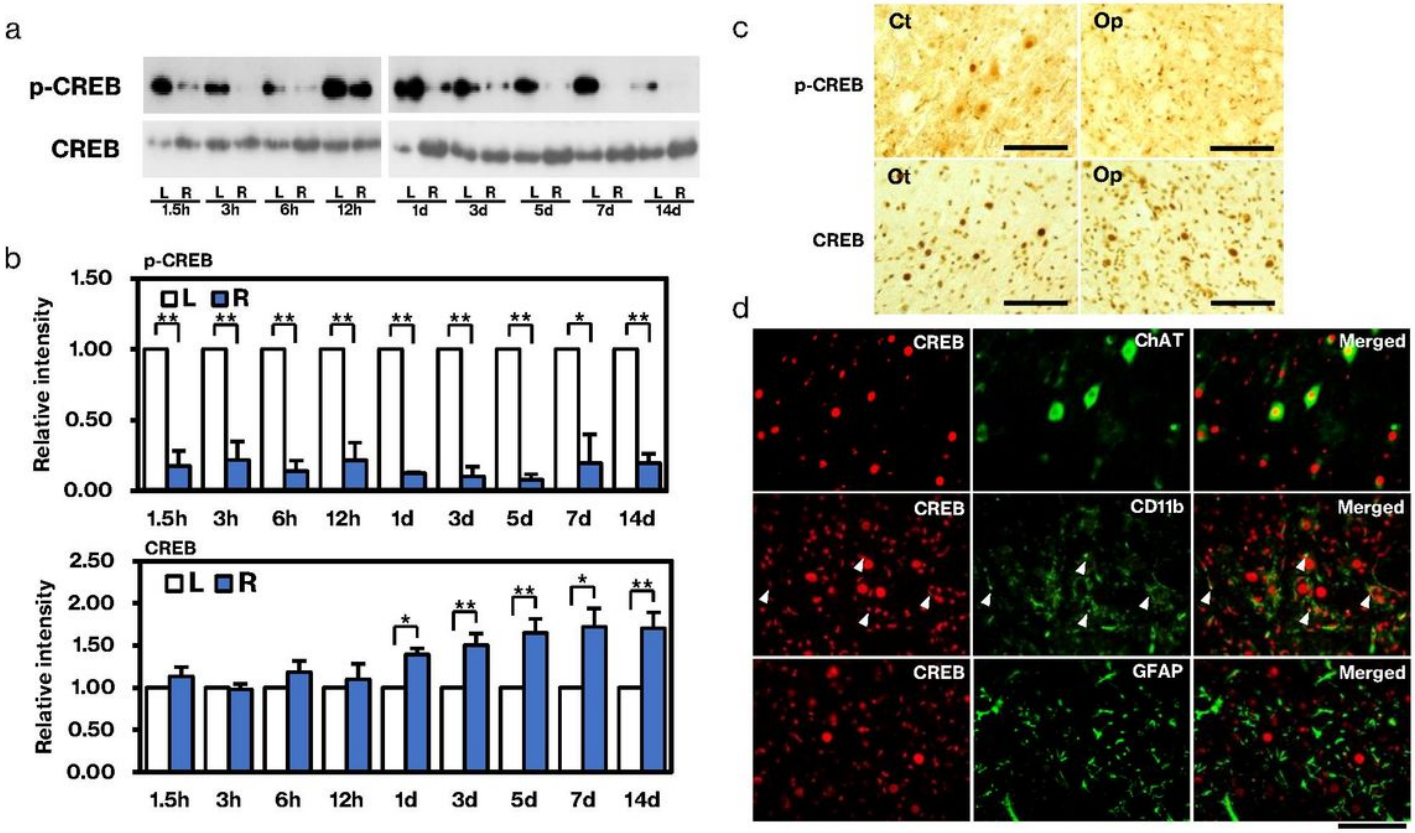


## Figure 4

### Changes of CREB in the axotomized facial nucleus

a. Immunoblot for p-CREB and CREB. Facial nucleus extracts taken at 1.5 h to 14 d post-injury were analyzed by immunoblot for p-CREB (p-CREB) and CREB (CREB). At each time point, the levels of p-CREB and CREB were compared between the contralateral (L) and ipsilateral (R) nuclei.

b. Quantitative analysis of p-CREB and CREB. The intensities of the p-CREB and CREB bands were determined by densitometry and were expressed as a value relative to that of the contralateral nucleus

(defined as 1.00). The data shown are means ± SDs from three to four independent experiments. Differences between the control nucleus (L) and operated nucleus (R) were assessed by Student's t-test (*P < 0.05, **P < 0.01).

c. Immunohistochemistry (ABC staining) for p-CREB (p-CREB) and CREB (CREB). Brainstem sections taken at 5 d post-insult were stained with anti-p-CREB antibody and anti-CREB antibody and the expression levels of p-CREB and CREB were compared between the control (Ct) and operated nucleus (Op). The scale bar is 100 μm.

d. Double staining with anti-CREB antibodies and motoneuron/glial markers. Brainstem sections were dually stained for CREB/ChAT, CREB/CD11b or CREB/GFAP. CREB was visualized by Alexa Fluor-568 (red), and ChAT, CD11b and GFAP antibody-positive cells were visualized by Alexa Fluor-488 (green). The merged image is shown on the right-hand side (Merged). The white arrowhead in the middle images indicates a CREB-positive nucleus. The scale bar is 100 μm.

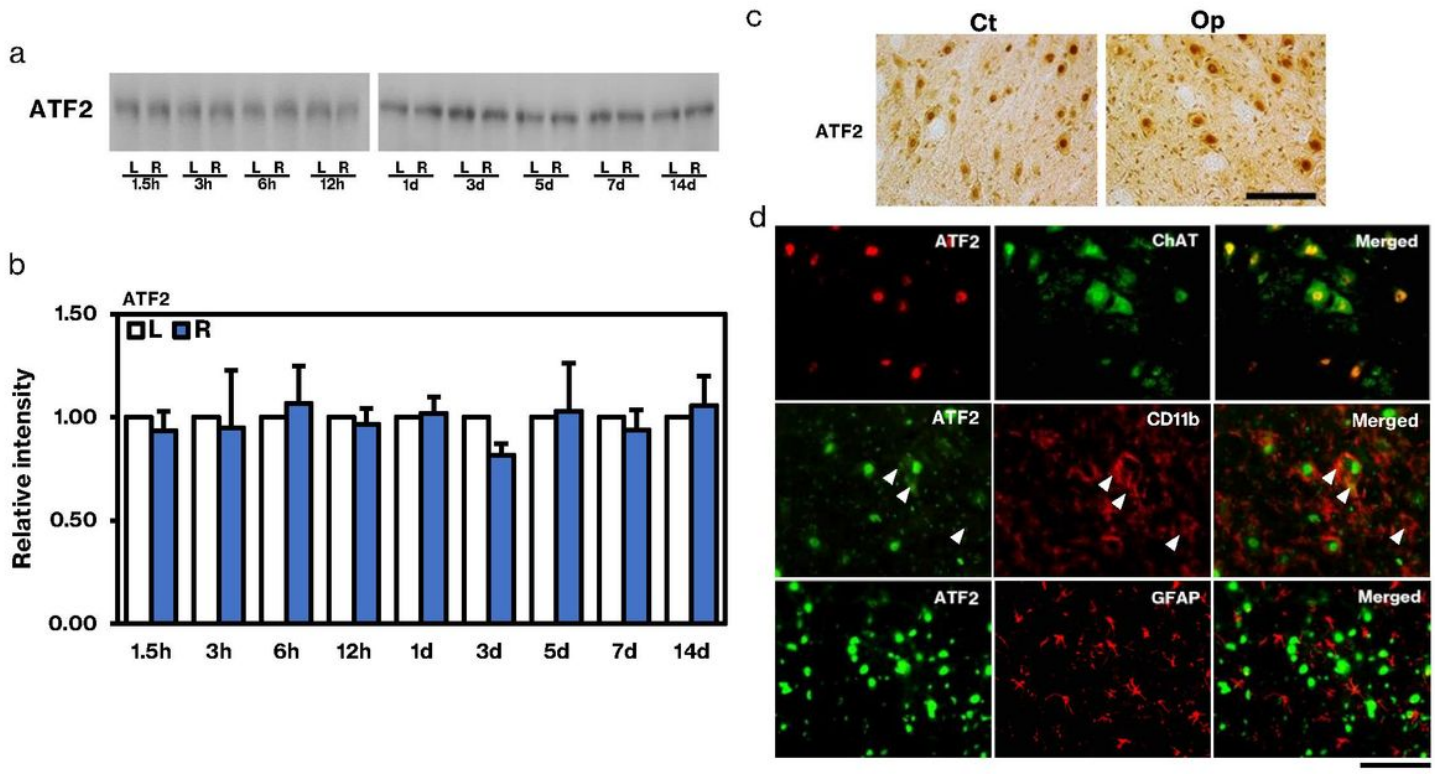


## Figure 5

### Changes of ATF2 in the axotomized facial nucleus

a. Immunoblot for ATF2. Facial nucleus extracts taken at 1.5 h to 14 d after injury were analyzed by immunoblotting for ATF2. At each time point, the control (L) and operated (R) nucleus were compared.

b. Quantitative analysis of ATF2. The intensities of the ATF2 bands were determined by densitometry and expressed as a value relative to that of the control nucleus (defined as 1.00). The data shown are means ± SDs from three independent experiments. Differences between the control nucleus (L) and operated nucleus (R) were assessed by Student's t-test (*P < 0.05, **P < 0.01).

c. Immunohistochemistry (ABC staining) for ATF2. Brainstem sections taken at 5 d post-injury were stained with anti-ATF2 antibody, and the levels of ATF2 were compared between control (Ct) and operated (Op) nuclei. The scale bar is 100 μm.

d. Immunohistochemistry for identifying ATF2-positive cells. Brainstem sections taken at 5d post-insult were dually stained with anti-ATF2/anti-ChAT antibodies, anti-ATF2/anti-CD11b antibodies or anti-ATF2/anti-GFAP antibodies. Anti-ATF2 antibody-positive cells were visualized by Alexa Fluor-568 (red) or Alexa Fluor-488 (green). ChAT and CD11b/GFAP were visualized by Alexa Fluor-488 (green) or Alexa Fluor-568 (red), respectively. The merged image is shown on the right-hand side (Merged). The white arrowheads in the middle images indicate small ATF2-positive nuclei. The scale bar is 100 μm.

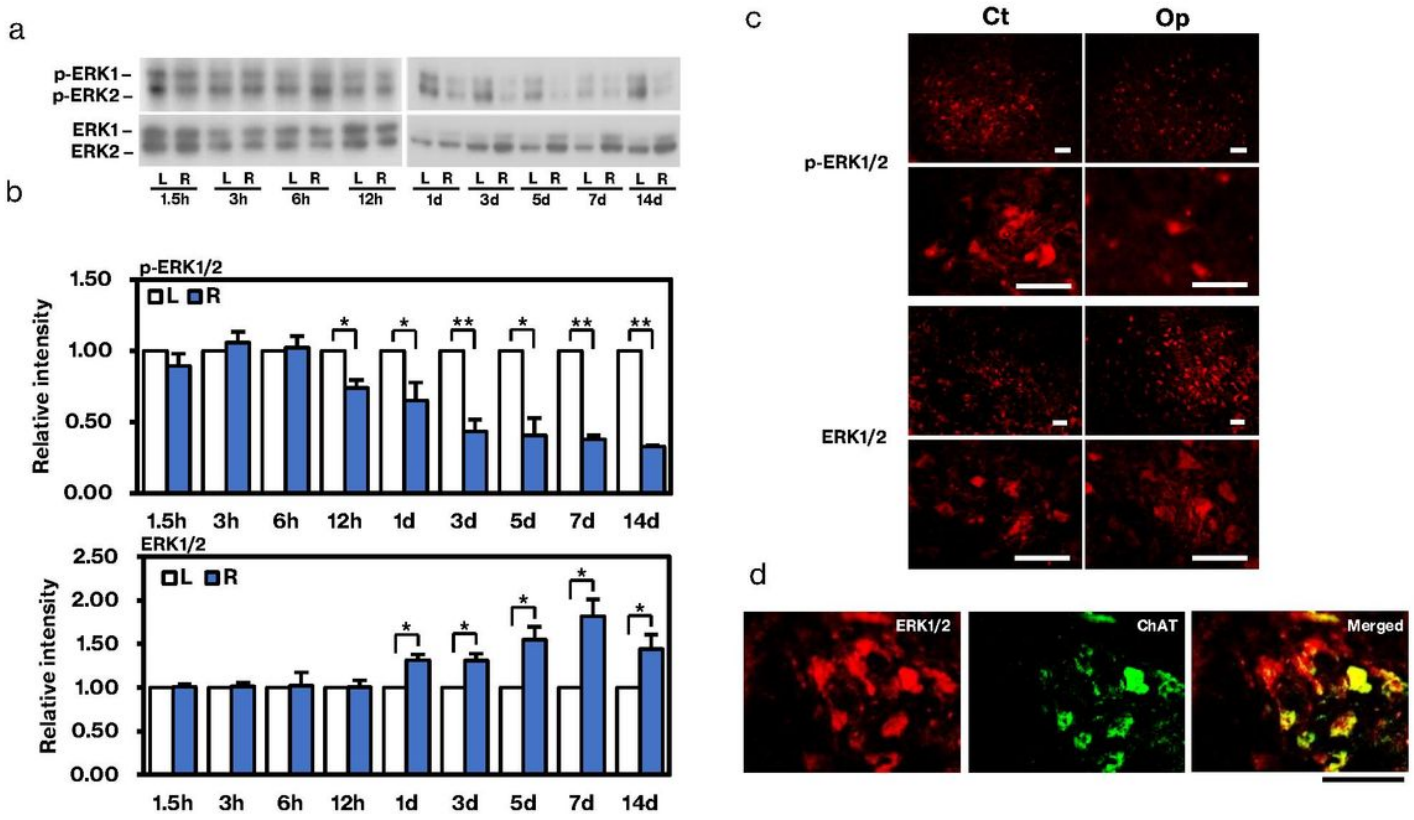


## Figure 6

### Changes of ERK1/2 in the axotomized facial nucleus

a. Immunoblot for p-ERK1/2 and ERK1/2. Facial nucleus extracts taken at 1.5 h to 14 d after injury were analyzed by immunoblot for p-ERK1/2 and ERK1/2. At each time point, the control (L) and operated (R) nucleus were compared.

b. Quantitative analysis of p-ERK1/2 and ERK1/2. The intensities of the p-ERK1/2 and ERK1/2 bands were determined by densitometry and expressed as a value relative to that of the control nucleus (defined as 1.00). The data shown are means ± SDs from three to four independent experiments. Differences between the control nucleus (L) and operated nucleus (R) were assessed by Student's t-test (*P < 0.05, **P < 0.01).

c. Immunohistochemistry for p-ERK1/2 and ERK1/2. Brainstem sections at 5 d post-injury were stained with anti-p-ERK1/2 or anti-ERK1/2 antibody, and the antibody levels were compared between the control (Ct) and operated (Op) nucleus. The scale bars are 100 μm.

d. Double staining for ERK1/2. Brainstem sections at 5 d post-insult were dually stained with anti-ERK1/2 antibody and anti-ChAT antibody. Anti-ERK1/2 antibody-positive cells (ERK1/2) and anti-ChAT antibody-positive cells (ChAT) were visualized by Alexa Fluor-568 (red) and Alexa Fluor-488 (green), respectively. The merged image is shown on the right-hand side (Merged). The scale bar is 100 μm.

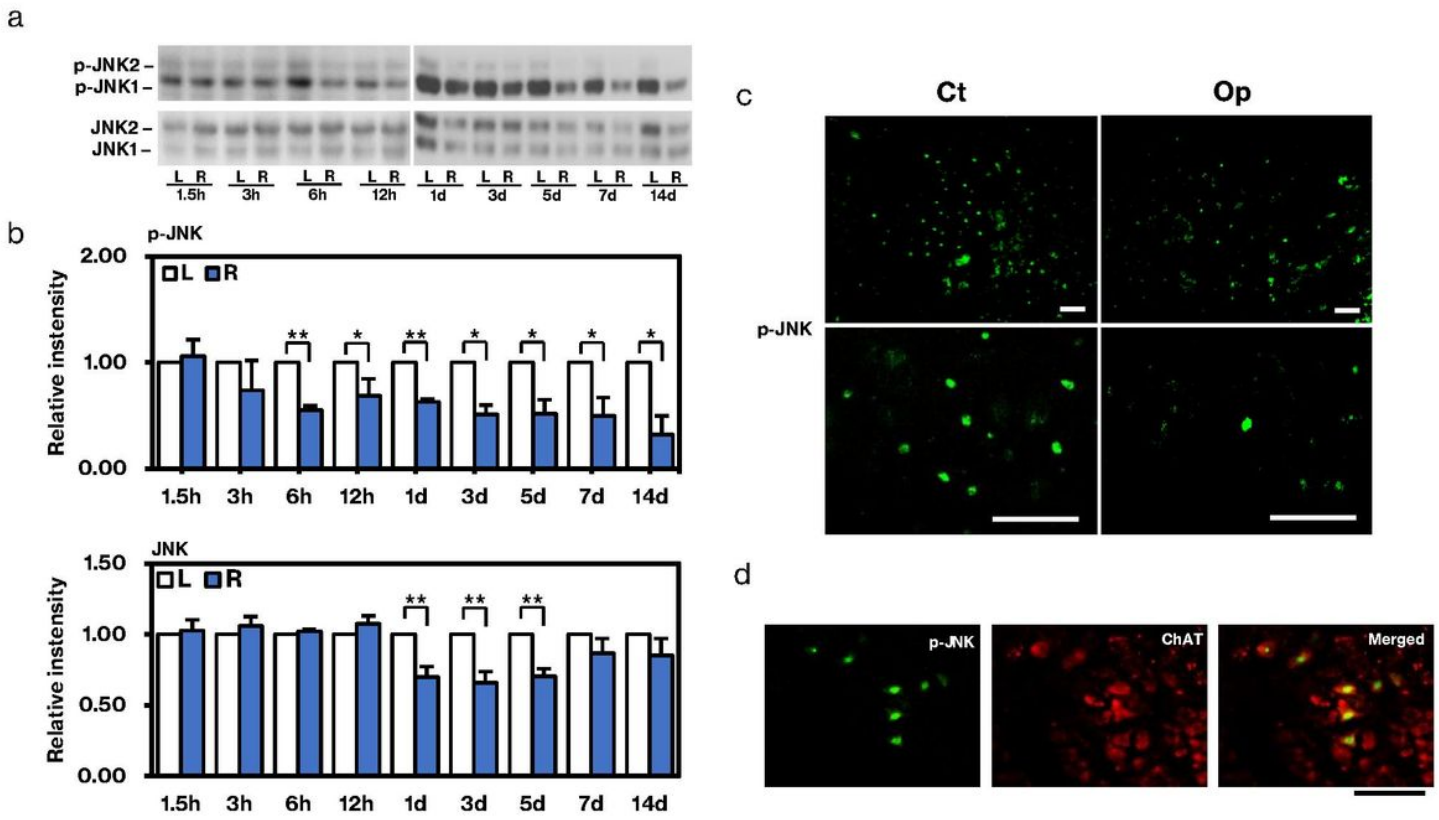


## Figure 7

### Changes of JNK in the axotomized facial nucleus

a. Immunoblot for p-JNK and JNK. Facial nucleus extracts taken at 1.5 h to 14 d after injury were analyzed by immunoblot for p-JNK and JNK. At each time point, the control (L) and operated (R) nucleus were compared.

b. Quantitative analysis of p-JNK and JNK. The intensities of the p-JNK and JNK bands were determined by densitometry and expressed as a value relative to that of the control nucleus (defined as 1.00) The data shown are means ± SDs from three to four independent experiments. Differences between the control nucleus (L) and operated nucleus (R) were assessed by Student's t-test (*P < 0.05, **P < 0.01).

c. Immunohistochemistry for p-JNK. Brainstem sections taken at 5 d post-insult were stained with anti-p-JNK antibody, and the control (Ct) and operated (Op) facial nucleus are shown. The scale bar is 100 μm.

d. Double staining with anti-p-JNK antibody and anti-ChAT antibody. Anti-p-JNK antibody-positive cells (p-JNK) and anti-ChAT antibody-positive cells (ChAT) were visualized by Alexa Fluor-488 (green) and Alexa Fluor-568 (red), respectively. The merged image is shown on the right-hand side (Merged). The scale bar is 100 μm.

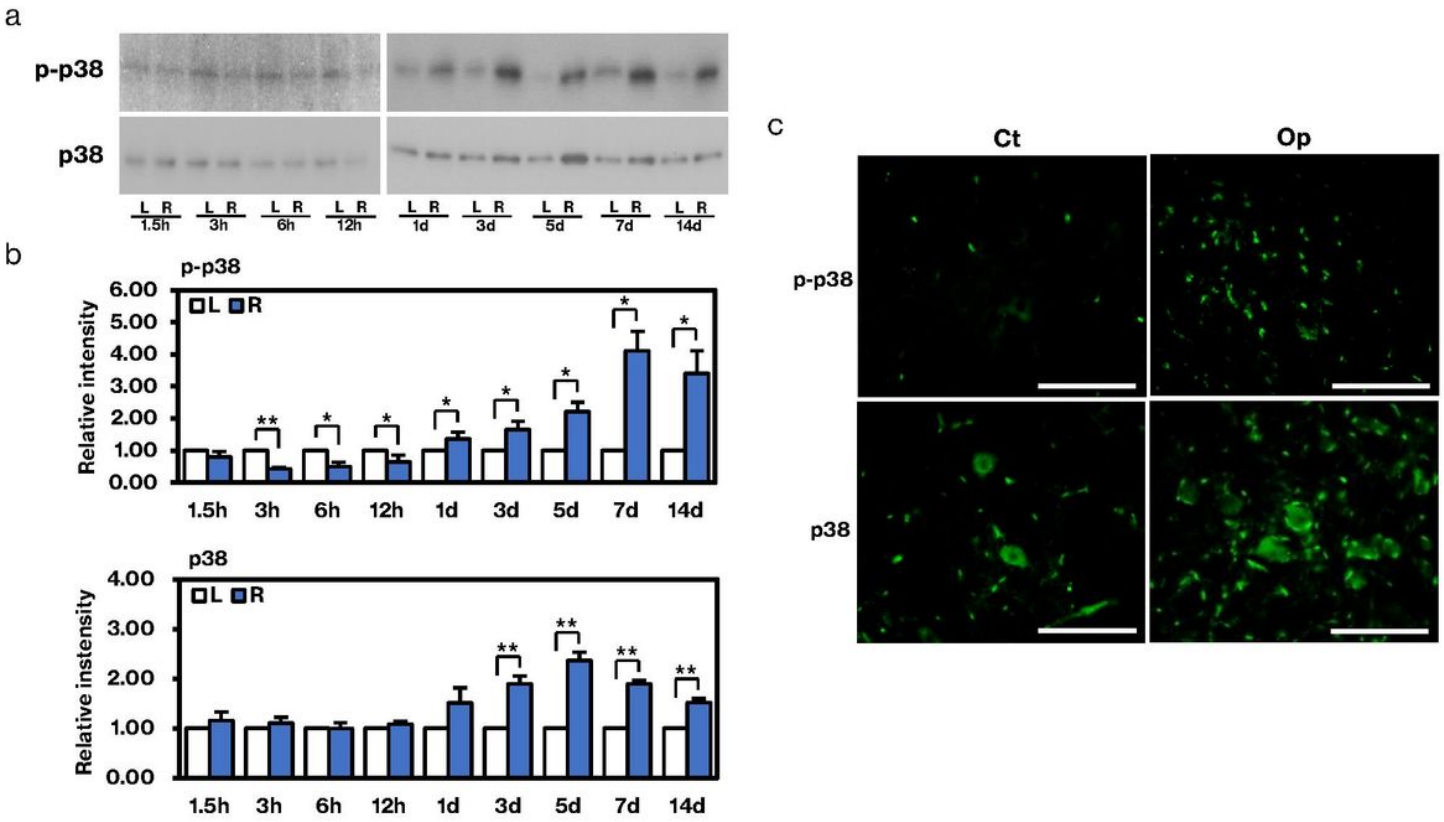


## Figure 8

## Changes of p38 in the axotomized facial nucleus

a. Immunoblot for p-p38 and p38. Facial nucleus extracts taken at 1.5 h to 14 d post-insult were analyzed by immunoblot for p-p38 and p38. At each time point, the control (L) and operated (R) nucleus were compared.

b. Quantitative analysis of p-p38 and p38. The intensities of the p-p38 and p38 bands were determined by densitometry and expressed as a value relative to that of the control nucleus (defined as 1.00). The data

shown are means ± SDs from three to five independent experiments. Differences between the control nucleus (L) and operated nucleus (R) were assessed by Student's t-test (*P < 0.05, **P < 0.01).

c. Immunohistochemistry for p-p38 and p38. Brainstem sections taken at 5 d post-insult were stained with anti-p-p38 antibody (p-p38) or anti-p38 antibody (p38), and the control (Ct) and operated (Op) facial nucleus were compared. The scale bar is 100 μm.

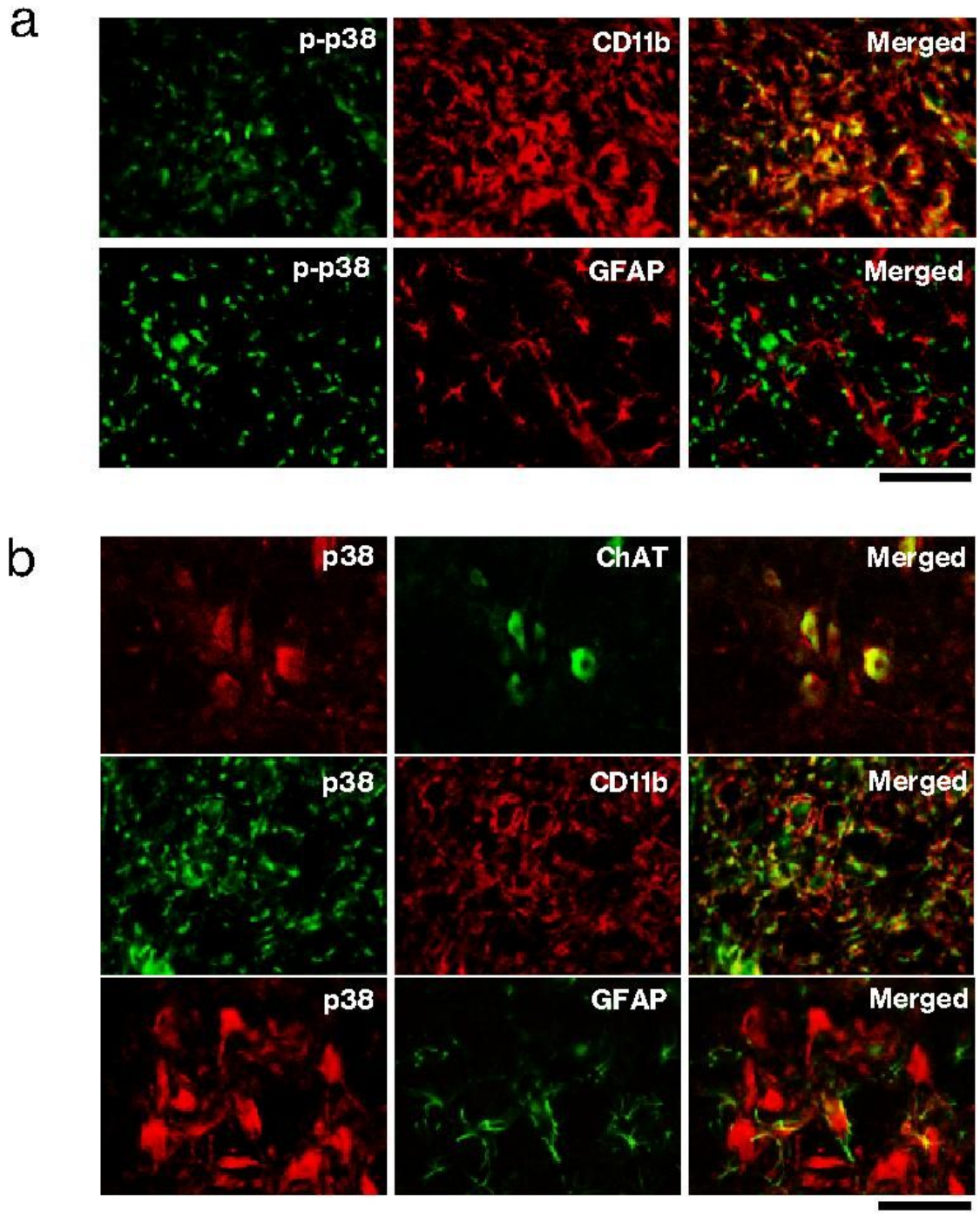

## Figure 9

### Immunohistochemistry for p-p38 and p38 in the axotomized facial nucleus.

a. Double staining for identifying p-p38-expressing cells. Brainstem sections taken at 5 d post-insult were dually stained with anti-p-p38 antibody/anti-CD11b antibody and anti-p-p38 antibody/anti-GFAP antibody. Anti-p-p38 antibody-positive cells and anti-GFAP antibody-positive cells were visualized by Alexa Fluor-488 (green) and Alexa Fluor-568 (red), respectively. The merged image is shown on the right-hand side (Merged). The scale bar is 100 μm.

b. Double staining for identifying anti-p38 antibody-positive cells. Brainstem sections taken at 5 d post-insult were dually stained with anti-p38/anti-ChAT, anti-p38/anti-CD11b or anti-p38/anti-GFAP antibodies. Anti-p38 antibody-positive cells were visualized by Alexa Fluor-568 (red) or Alexa Fluor-488 (green). Anti-ChAT antibody-positive cells were visualized by Alexa Fluor-488 (green). Anti-CD11b antibody-positive cells were visualized by Alexa Fluor-594 (red). Anti-GFAP antibody-positive cells were visualized by Alexa Fluor-488 (green). The merged image is shown on the right-hand side (Merged). The scale bar is 100 μm.

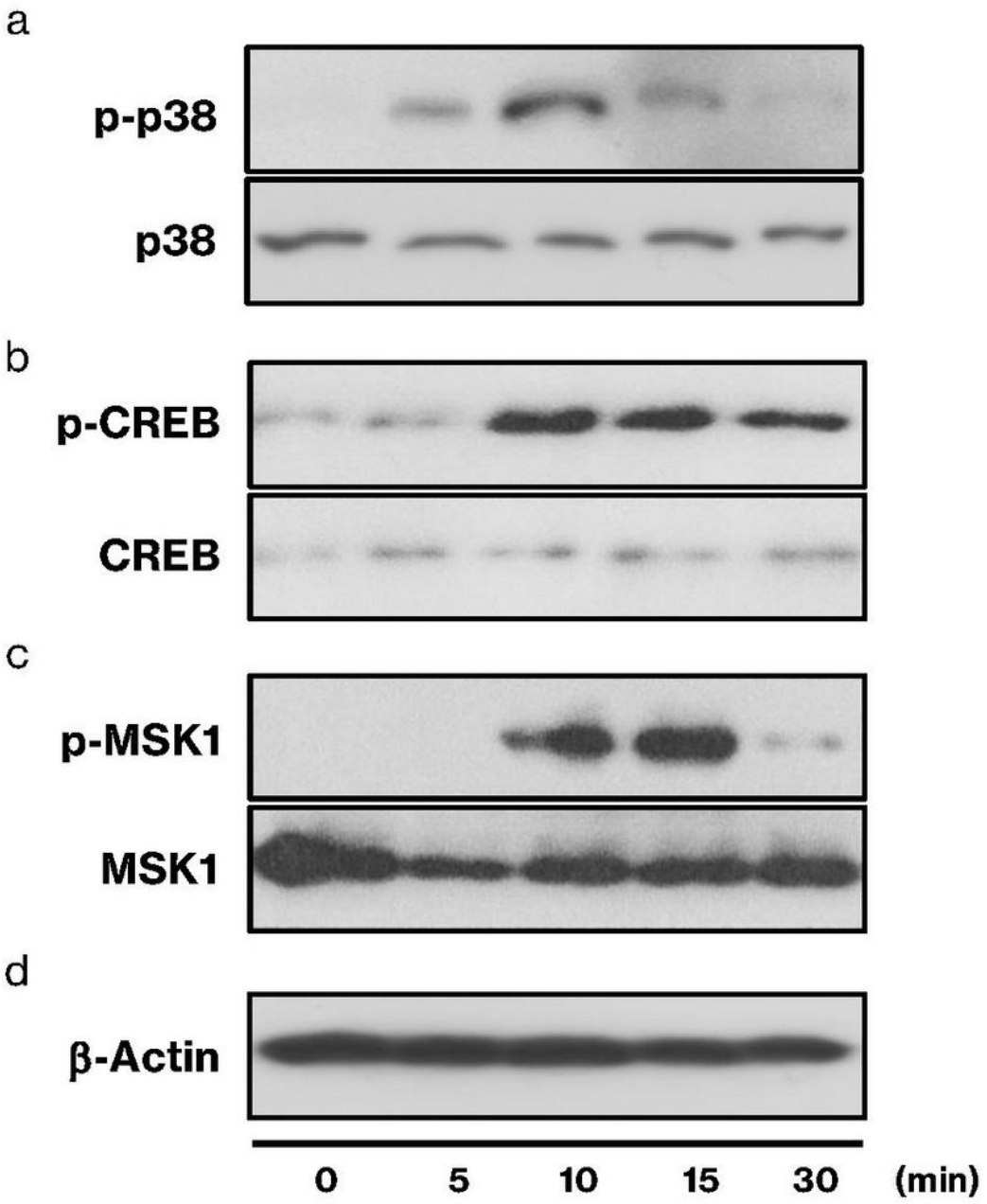


Figure 10

Activation of p38, CREB and MSK1 in M-CSF stimulated microglia

a, b, c, d. Analysis of p-p38/p38, p-CREB/CREB, p-MSK1/MSK1 and b-actin. Five microglial cultures were prepared, and exposed to M-CSF (20 ng/mL). Microglia were recovered at 0, 5, 10, 15 and 30 min after M-

CSF stimulation, and analyzed by immunoblot for p-p38/p38 (a), p-CREB/CREB (b), p-MSK1/MSK1 (c) and b-Actin (d).

## Supplementary Files

This is a list of supplementary files associated with this preprint. Click to download.

- NResTable1.docx